Optics Letters

Low-power microelectromechanically tunable silicon photonic ring resonator add–drop filter

CARLOS ERRANDO-HERRANZ, FRANK NIKLAUS, GÖRAN STEMME, AND KRISTINN B. GYLFASON*

Micro and Nanosystems, KTH Royal Institute of Technology, Osquldas väg 10, SE-100 44 Stockholm, Sweden
*Corresponding author: kristinn.gylfason@ee.kth.se

Received 9 June 2015; accepted 3 July 2015; posted 9 July 2015 (Doc. ID 241885); published 24 July 2015

We experimentally demonstrate a microelectromechanically (MEMS) tunable photonic ring resonator add–drop filter, fabricated in a simple silicon-on-insulator (SOI) based process. The device uses electrostatic parallel plate actuation to perturb the evanescent field of a silicon waveguide, and achieves a 530 pm resonance wavelength tuning, i.e., more than a fourfold improvement compared to previous MEMS tunable ring resonator add–drop filters. Moreover, our device has a static power consumption below 100 nW, and a tuning rate of –62 pm/V, i.e., the highest reported rate for electrostatic tuning of ring resonator add–drop filters. © 2015 Optical Society of America

OCIS codes: (130.3120) Integrated optics devices; (130.4815) Optical switching devices; (130.7408) Wavelength filtering devices; (070.5753) Resonators; (220.4610) Optical fabrication; (230.4685) Optical microelectromechanical devices.

http://dx.doi.org/10.1364/OL.40.003556

Ring resonators are key components of silicon photonics due to their small footprint and ability to filter and route narrowband signals. The rings show standing wave resonances when the optical path length of the ring waveguide is a multiple of the excitation wavelength. Thus, by changing the optical length of the ring, e.g., by perturbing the effective refractive index of the waveguide mode, one can tune the resonance wavelength. Tunable ring resonators find applications in integrated optical networks that require selection or dynamic tuning of wavelength channels. Examples of such applications include drift compensation of wavelength division multiplexers (WDMs) [1], optical wavelength routers [2] including reconfigurable optical add–drop multiplexers (ROADMs) [3], broadband switches [4], four-wave mixers [5], waveguide mirrors [6], optical angular momentum emitters [7], and tunable lasers [8]. Most of these applications require densely packed high-Q rings that are able to add and drop down to 50 GHz channels, with wavelength tuning spanning a number of channels. Moreover, such applications require ring resonators with independent tuning, i.e., low cross-talk between adjacent devices.

Ring resonators tuned by free-carrier injection have achieved high-speed tuning [9]. However, free-carrier absorption results in high optical loss and short wavelength shift, which limits their usefulness for add–drop applications. Thermo-optic tuning of ring resonators has shown large wavelength shift with low optical loss [10], but high power consumption and thermal cross-talk between neighboring devices hamper its applicability in densely integrated optical interconnects [11]. Integration of electro-optic materials with low static power dissipation have so far shown low tuning effects, high driving voltages, and optical interference due to fabrication complexity [12]. Table 1 summarizes reported performance of tunable ring resonator add–drop filters.

MEMS tunable ring resonators are good candidates for wavelength selection in optical networks due to their low static power dissipation and high optical Q. Such filters have already shown low-power wavelength tuning [14], but since the tuning mechanism was based on deflecting a deposited cantilever on

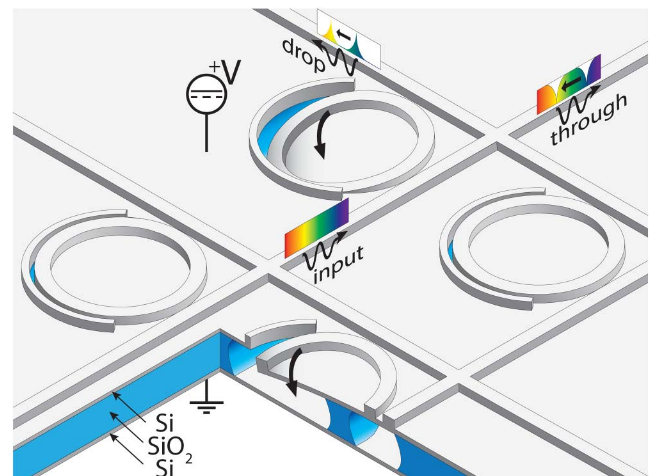

Fig. 1. Most applications of tunable add–drop filters require a large number of densely packed devices with low cross-talk. Here, we demonstrate a low-power MEMS tunable add–drop filter fabricated by a simple SOI-based process. Parallel plate actuation of a free-standing cantilever that contains the ring resonator waveguide changes the waveguide geometry. This affects the effective refractive index of the resonant optical mode, resulting in a shift of resonance wavelength.

0146-9592/15/153556-04$15/0$15.00 © 2015 Optical Society of America

Table 1. Reported Performance of Tunable Add–Drop Filters Based on Ring Resonators Working at a Wavelength of 1550 nm[a]

Tuning mechanism	FSR [nm]	BW [nm]	$\Delta\lambda_{max}$ [nm]	$\frac{\partial\lambda}{\partial P}$ [$\frac{nm}{mW}$]	$\frac{\partial\lambda}{\partial V}$ [$\frac{pm}{V}$]	P_{static} [nW]	ER_T [dB]	ER_D [dB]	IL [dB]	# masks	# dep./impl.	Ref.
Carrier injection	3.5	0.5	0.56	0.58		10^6	11	13	7	3	3	[9]
Thermo-optic	35	0.9	35	1.8		10^7	10	18	7	4	3	[13]
Thermo-optic	19	0.2	19	0.9		10^7		25		4	4	[10]
Electro-optic	2.7	0.5	0.67		1.1	$<10^2$	17.5			4	4	[12]
MEMS	6.6	0.2	0.12		−14	$<10^2$	20	23	5	2	4	[14]
MEMS	1.2	0.16	0.53		−62	$<10^2$	7	15	8	2	0	This work

[a] In terms of: free spectral range (FSR), −3 dB bandwidth (BW), maximum resonance shift ($\Delta\lambda_{max}$), tuning rate ($\frac{\partial\lambda}{\partial P}$ or $\frac{\partial\lambda}{\partial V}$), static power consumption at maximum tuning (P_{static}), extinction ratios for through and drop ports (ER_T and ER_D), insertion loss to drop port (IL), number of lithography masks (# masks), and number of deposited or implanted layers (# Dep./Impl).

top of a ring resonator, it resulted in a short wavelength shift of 122 pm. In previous work, we presented a novel ring resonator tuning principle applied to a notch filter that resulted in good optical performance and significant tuning [15,16]. These devices, along with other MEMS tunable notch filters with large tuning [17], had no drop port, which is a requirement for optical networks and nontrivial to implement in many previously demonstrated technologies.

Here, we demonstrate an MEMS tunable add–drop filter (Fig. 1) fabricated using a silicon-on-insulator (SOI) wafer. We use an integrated electrostatic actuator to perturb the evanescent field of a silicon ring resonator and shift its resonance wavelength.

Figure 2 shows results from a simulation of a waveguide optical mode, performed with a finite element method eigenmode solver (COMSOL Multiphysics v4.4), and the effect of vertical displacement of the ring waveguide (from 0.2 μm above down to 0.4 μm below the static silicon rim) on the effective mode index. Displacement of the waveguide toward the static silicon rim results in increased optical power propagating through silicon rather than through air, and increased mode index, which translates into redshift of the ring's resonance wavelength. Conversely, displacement away from the rim results in blueshift, until the mode is far enough away not to be affected by the static silicon rim.

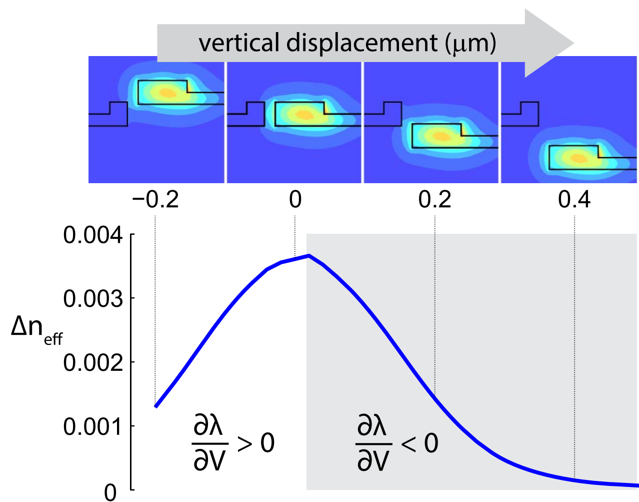

Fig. 2. FEM eigenmode simulations show the effect of vertical displacement of the ring resonator waveguide in relation to the static silicon rim on the effective mode index. Electrostatic actuation with a voltage V results in downward movement of the waveguide, which thus translates into redshift ($\frac{\partial\lambda}{\partial V} > 0$) of the resonance wavelength of the ring resonator as the waveguide approaches the static rim, and blueshift ($\frac{\partial\lambda}{\partial V} < 0$, shaded area) as the waveguide moves away from it.

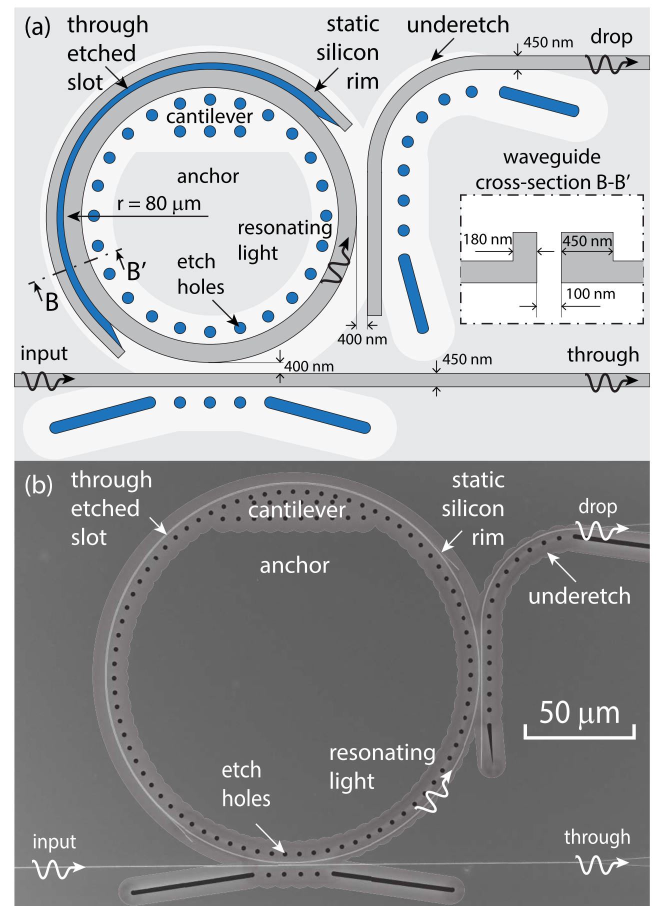

Fig. 3. (a) Top view schematic and (b) SEM of the MEMS tunable ring resonator add–drop filter. Light couples from the input waveguide into the ring waveguide, half of which is encircled by a static silicon rim separated by a through etched slot. A suspended cantilever is formed by the slot and the etch holes. Tuning is achieved by electrostatic actuation of the cantilever by an applied voltage, and the resonance wavelength shift is detected at the through and the drop ports.

Figure 3(a) shows a schematic of our MEMS tunable add–drop filter. The device was fabricated by patterning an e-beam lithography mask on a standard SOI photonics substrate (220 nm thick silicon device layer and 2 μm buried oxide). Following a timed silicon dry etch to form the waveguides, a second e-beam mask was patterned. Then, a second dry etch through the silicon device layer forms etch holes and a slot. After a final release-etch of the buried oxide layer in hydrofluoric acid (HF) and critical point drying, the through etched slot and etch holes define a suspended silicon cantilever. A SEM image of a fabricated device is shown in Fig. 3(b). The fabrication details have been reported in [15].

For device characterization, transverse electric (TE) polarized light was coupled in and out of the chip through optical fibers aligned to on-chip grating couplers, and the light transmitted from the through and drop ports was measured by a wavelength domain component analyzer (Agilent Technologies 86082A). Figure 4(a) shows the optical power transmitted in the wavelength range from 1536 to 1553 nm, with extinction ratios of 7 and 15 dB for the through and drop ports, respectively, and 8 dB insertion loss to drop port. For electrostatic tuning, an actuation voltage was applied between the grounded silicon base and the device layer of the SOI chip by direct contact of a compliant probe needle. The tuning of the transmitted spectra by applying a voltage from 0 up to 21.5 V is shown in Fig. 4(b). The tuning effect on the resonance wavelength, FSR, and BW of the drop port transmission is shown in Fig. 5. As seen in Fig. 5(a), the device shows a maximum resonance shift of 530 pm (64 GHz). For actuation voltages below 12 V, the device showed a redshift and a nonlinear tuning rate. As indicated by our simulation in Fig. 2, and by microscope inspection, this is most likely caused by a static deflection of the cantilever out of the device plane, due to relaxation of stress in the released silicon device layer. After the cantilever reaches the zero-deflection plane at 12 V, further actuation results in blueshift in the range from 12 to 21.5 V. We observe a linear −62 pm/V (7.6 GHz/V) tuning rate, which is the highest value reported for electrostatically tuned ring resonator based add–drop filters. The observed zero-drift in Fig. 5(a) is most likely caused by charge trapping in the device layer, and could be reduced by alternating the polarity of the actuation voltage [18]. From Fig. 5(b), we observe an average FSR of 1176 pm (148 GHz), which varies by less than 1 pm over the full tuning range, and from Fig. 5(c), an average BW of 160 pm (20 GHz), which at 1544 nm equates to a Q of 10^4. The BW drop above 15 V, seen in Fig. 5(c), is most likely caused by a reduction in scattering loss, since the mode has less overlap with the rough etched sidewalls of the slot at large displacements.

Table 1 compares our results to other ring resonator based tunable add–drop filters. Thermo-optically tuned rings show larger FSR and tuning range [10,13], at the cost of a power dissipation at least four orders of magnitude above that of electrostatically tuned rings. High power dissipation is also an issue for carrier injection tuning [9], combined with carrier absorption, that results in a three times larger BW. Among the low-power devices, the integration of electro-optic materials [12] requires complex fabrication, resulting in a three times larger BW, due to scattering losses. The high driving voltage up to 600 V resulted in a tuning rate that is 50 times lower than in our device, while having a comparable tuning range. Compared to other MEMS actuated rings [14], our device

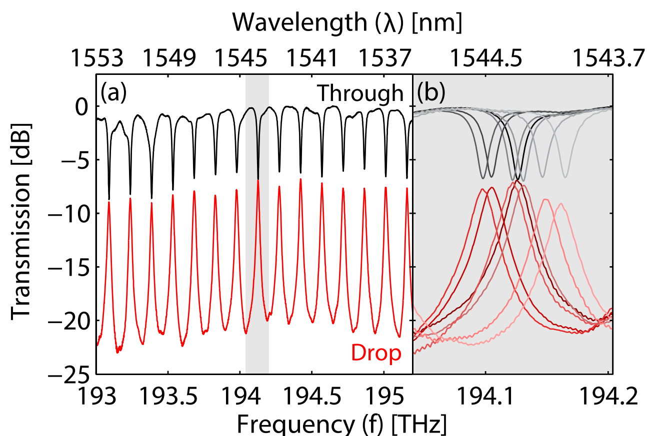

Fig. 4. (a) Transmission spectra at the through and drop ports of the device in Fig. 3(b). (b) An enlarged view of the shaded area in (a), showing the movement of the spectra under actuation voltages between 0 and 21.5 V. The saturation of the line color decreases with voltage.

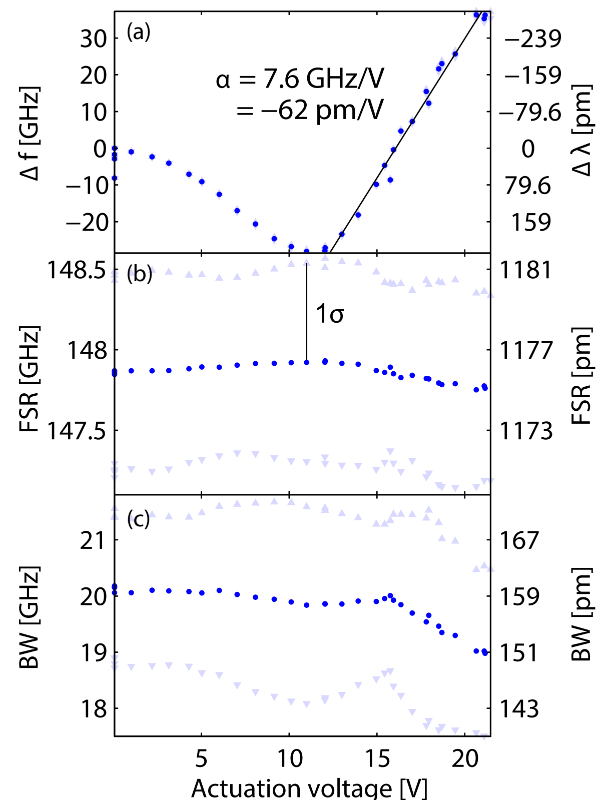

Fig. 5. (a) Resonance shift, (b) free spectral range (FSR), and (c) −3 dB bandwidth (BW) of the MEMS tunable add–drop filter, under actuation voltages from 0 to 21.5 V. The data is from the drop port spectra and averaged over the 15 resonances shown in Fig. 4. The triangles indicate one standard deviation (1σ). The device presents a maximum resonance shift of 530 pm with a linear tuning rate of 7.6 GHz/V (−62 pm/V) for actuation voltages between 12 and 21.5 V.

presents a comparable BW and a more than fourfold increase in tuning range and tuning rate. However, a lack of fine optimization of the coupling gap of the ring caused our device to show the lowest extinction ratios and highest insertion loss, which was, based on our previous experience, most likely caused by fabrication variations of the coupling gap. Fabrication variations also affected the waveguide roughness and slot width, resulting in an increase in BW and a decrease in tuning range compared to the first report of our tuning principle [15]. However, improved lithography alignment resulted in a higher tuning rate, due to the avoidance of any silicon residues bridging the waveguide slot.

We believe the presented results are a promising step toward future integration of optical networks. However, a number of improvements are required for WDM and ROADM applications in telecommunications, where the tuning range needs to span the whole C-band. This could be achieved with the presented technology by using the Vernier effect on cascaded rings [19], but a larger tuning range of a single ring is still preferred. This can be realized by reducing the ring size (already demonstrated in [16]) and increasing the tuning effect. A larger tuning effect can in principle be achieved by (i) displacing a larger fraction of the ring waveguide, (ii) reducing the slab thickness, or (iii) reducing the ring waveguide width, which will require tighter control over fabrication processes such as the silicon dry etch and lithography. The extinction ratios and insertion loss can be improved by optimization of the coupling gap.

In conclusion, we have demonstrated a MEMS tunable photonic ring resonator add–drop filter with a low static power drain, good optical performance, and a high tuning rate. Moreover, the very simple fabrication process facilitates integration with other optical components, and is compatible with high-volume production.

Funding. European Research Council (ERC) (267528, 277879); Vetenskapsrådet (Swedish Research Council) (621-2012-5364).

Acknowledgment. The authors thank Dr. Xi Chen and Prof. Lech Wosinski at the KTH ICT school for help with the characterization setup.

REFERENCES

1. D. Sadot and E. Boimovich, IEEE Commun. Mag. **36**(12), 50 (1998).
2. N. Sherwood-Droz, H. Wang, L. Chen, B. G. Lee, A. Biberman, K. Bergman, and M. Lipson, Opt. Express **16**, 15915 (2008).
3. E. J. Klein, D. H. Geuzebroek, H. Kelderman, G. Sengo, N. Baker, and A. Driessen, IEEE Photon. Technol. Lett. **17**, 2358 (2005).
4. Y. Vlasov, W. M. J. Green, and F. Xia, Nat. Photonics **2**, 242 (2008).
5. X. Zeng, C. M. Gentry, and M. A. Popović, Opt. Lett. **40**, 2120 (2015).
6. J. K. S. Poon, J. Scheuer, and A. Yariv, IEEE Photon. Technol. Lett. **16**, 1331 (2004).
7. M. J. Strain, X. Cai, J. Wang, J. Zhu, D. B. Phillips, L. Chen, M. Lopez-Garcia, J. L. O'Brien, M. G. Thompson, M. Sorel, and S. Yu, Nat. Commun. **5**, 4856 (2014).
8. H. Rong, S. Xu, Y.-H. Kuo, V. Sih, O. Cohen, O. Raday, and M. Paniccia, Nat. Photonics **1**, 232 (2007).
9. A. W. Poon, X. Luo, F. Xu, and H. Chen, Proc. IEEE **97**, 1216 (2009).
10. P. Dong, W. Qian, H. Liang, R. Shafiiha, N.-N. Feng, D. Feng, X. Zheng, A. V. Krishnamoorthy, and M. Asghari, Opt. Express **18**, 9852 (2010).
11. D. A. B. Miller, Proc. IEEE **97**, 1166 (2009).
12. J. Takayesu, M. Hochberg, T. Baehr-Jones, E. Chan, G. Wang, P. Sullivan, Y. Liao, J. Davies, L. Dalton, A. Scherer, and W. Krug, J. Lightwave Technol. **27**, 440 (2009).
13. M. R. Watts, W. Zortman, D. C. Trotter, G. N. Nielson, D. L. Luck, and R. W. Young, *Conference on Lasers and Electro-Optics/International Quantum Electronics Conference* (IEEE, 2009), paper CPDB10.
14. S. M. C. Abdulla, L. J. Kauppinen, M. Dijkstra, M. J. de Boer, E. Berenschot, H. V. Jansen, R. M. de Ridder, and G. J. M. Krijnen, Opt. Express **19**, 15864 (2011).
15. C. Errando-Herranz, F. Niklaus, G. Stemme, and K. B. Gylfason, *Conference on Micro Electro Mechanical Systems* (IEEE, 2015), p. 53.
16. C. Errando-Herranz, F. Niklaus, G. Stemme, and K. B. Gylfason, *Transducers* (IEEE, 2015), p. 1001.
17. H. M. Chu and K. Hane, IEEE Photon. Technol. Lett. **26**, 1411 (2014).
18. J. Wibbeler, G. Pfeifer, and M. Hietschold, Sens. Actuators A **71**, 74 (1998).
19. P. Urquhart, J. Opt. Soc. Am. A **5**, 803 (1988).